Chemical Physics 145 (1990) 219–238
North-Holland

Experimental and theoretical studies of simple attractive Penning ionization systems

A. MERZ, M.W. MÜLLER, M.-W. RUF, H. HOTOP
Fachbereich Physik, Universität Kaiserslautern, 6750 Kaiserslautern, FRG

W. MAYER and M. MOVRE [1]
Fachbereich Chemie, Universität Kaiserslautern, 6750 Kaiserslautern, FRG

Received 18 December 1989

Quantum mechanical calculations based on local complex potential theory and ab initio potential data are presented for the Penning ionization systems $He^*(2\,^3S)+H$, Li, Na, and $He^*(2\,^1S)+Na$. The dependence of the electron energy spectrum on the complex entrance channel potential and on the collision energy is shown within the "$\Delta J \equiv J_+ - J_* = 0$" approximation (i.e. conservation of the heavy particle angular momentum upon electron emission). Further calculations demonstrate the more detailed structure of the electron spectra if a selected number of heavy particle partial waves is considered only. High resolution, angular dependent electron spectrometric studies of the systems He^*+Li, Na show the need to take angular momentum transfer ($\Delta J \neq 0$) into account. The new experimental results are discussed in connection with earlier work, and quantal model calculations with the inclusion of rotational energy transfer illustrate how the angular dependence of the electron spectra can be qualitatively understood in terms of a recently given semiclassical model.

1. Introduction

Studies of the energy spectrum of electrons emitted in thermal collisions of excited rare gas atoms A^* with target atoms X (Penning ionization)

$$A^* + X \rightarrow A + X^+ + e^-(\epsilon) ,$$

have provided detailed information on the physics of these inelastic processes, in particular on the interaction potentials of attractive systems (well depth D_e^* of A^*+X interaction potential large compared with collision energy E_{rel}) [1–6]. Following the semiclassical description of the electron energy spectrum [7] it is possible to determine the well depth of the real part $V_*(R)$ of the local complex entrance channel potential $V_c(R) = V_*(R) - i\Gamma(R)/2$ through an Airy analysis of the low energy part of the electron energy distribution. In addition the autoionization width function $\Gamma(R)$, i.e. the imaginary part of the entrance potential, has usually been determined in a semi-empirical way be establishing satisfactory agreement between the measured spectrum and quantum mechanical fit calculations [8,9].

In these comparisons, it was assumed that the electron energy spectrum measured at a specific angle θ with respect to the relative collision velocity (usually at $\theta = 90°$ by sampling electrons in a direction perpendicular to the plane defined by the two orthogonal atomic beams) is representative for an angle-integrated spectrum. Moreover, all the numerical work has been done on the basis of approximations, which effectively mean angular momentum conservation for the heavy particle system in the transition from the entrance channel (J_*) to the ionic system (J_+) [8–14]. Consequently, all emitted electron are treated as being of s character.

In this paper, we present new results of experimental and theoretical investigations of the attractive Penning systems $He^*(2\,^3S)+H$, Li, Na, and $He^*(2\,^1S)+Na$, carried out with the aim to obtain improved insight into the physics of these elementary autoionizing quasi-molecules and to provide perspectives for future experiments. In section 2, we

---

[1] Permanent address: Institute of Physics of the University, 4100 Zagreb, Yugoslavia.

0301-0104/90/$ 03.50 © 1990 – Elsevier Science Publishers B.V. (North-Holland)

briefly discuss the approximations pertinent in the theoretical formulation. In section 3, we demonstrate the influence of different input parameters (autoionization width $\Gamma(R)$, collision energy E_{rel}, number of contributing heavy particle partial waves etc.) on the quantum mechanically calculated electron energy spectrum. Especially for the case of $\mathrm{He}^*(2\,^3\mathrm{S})+\mathrm{H}$ we extend the model calculations of an earlier work [9] and critically analyze the degree of understanding we have achieved by now (section 3.1).

Although approximate, model calculations for angle-integrated spectra done within the $\Delta J \equiv J_+ - J_* = 0$ restriction are sufficient to illustrate the J-composition of Penning electron spectra as well as their dependence on the underlying potentials and on collision energy (note that we use simply J for the angular momentum of the heavy particle system, when we assume $J_* = J_+ \equiv J$, in the text and in the figures). If potentials are not a priori known from theory, model fit calculations may serve to provide fairly detailed information [8,9], but – as will be seen – there are severe limitations especially with respect to the autoionization width; this is partially due to experimental uncertainties and approximations in the theoretical description, but mainly connected with the intricate way, in which the width enters into the electron energy spectrum.

An essential step forward in the interpretation of the electron spectra and towards a deeper understanding of the Penning process was achieved through the availability and application of accurate ab initio potentials including the ionization width function [13,15], so that quantal fit calculations could be replaced by ab initio ones.

Differences between our ab initio results [15] and the available experimental data [16] motivated us to study the simple Penning ionization systems $\mathrm{He}^*+\mathrm{Li}$, Na again with a different experimental setup [13]. In contrast to the earlier measurements, where electrons were detected at right angles to the direction of the two orthogonal atomic beams [8,9,16], a cylindrical mirror electron spectrometer was used to detect electrons emitted into a $\Delta\varphi = 2\pi$ cone. In a second step the acceptance range of the spectrometer was reduced to limited $\Delta\varphi = 70°$ sections, so that electron energy spectra could be recorded under different emission angles θ with respect to the relative velocity vector $v_{\mathrm{rel}} = v_{\mathrm{A}^*} - v_{\mathrm{X}}$.

In section 3.2 we compare an angle integrated spectrum for $\mathrm{He}^*+\mathrm{Na}$ with an e^- distribution measured under $\theta = 90 \pm 25°$, which confirms the angular dependence of the electron spectrum previously reported for the similar systems $\mathrm{He}^*+\mathrm{Li}$ [13]. In addition, we discuss the new experimental results in connection with the earlier work of Ruf et al. [16] and the theoretical study of Padial et al. [14].

In section 3.3 we extend the angle-dependent e^- spectra for $\mathrm{He}^*+\mathrm{Li}$ [13] to five different detection angles and pursue further the discussion given earlier [13] on the explanation of the angular dependence of the electron energy spectrum by considering $\Delta J \neq 0$ processes.

2. Theory

2.1. The determination of well depths from Penning electron spectra

As already mentioned above, one of the purposes for recording Penning ionization electron spectra is to determine the well depth of the entrance channel potential from the low energy edge position of the electron energy distribution. Several authors have developed semiclassical descriptions of the electron energy spectrum [7,17–20]. The essential formulae for Penning ionization were first given by Miller [7]; he assumed the validity of local (complex) potentials as well as electronic energy conservation

$$\epsilon(R) = V_*(R) - V_+(R) \equiv \Delta V(R)\,, \tag{1}$$

together with the neglect of angular momentum changes in the ionization process, i.e.

$$\Delta J \equiv J_+ - J_* = 0\,. \tag{2}$$

For the electron energy distribution near the minimum of the difference potential ($\hat{\epsilon} \equiv \epsilon(\hat{R})$; $\hat{R}$ = distance, where the difference potential is minimal) he derived a simple equation with the following S-matrix element:

$$S^J_{\mathrm{f}\leftarrow\mathrm{i}} \propto \cos(\tau)\ \mathrm{Ai}(z)\,, \tag{3}$$

with

$$z = \left(\frac{2\mu^2}{\hbar^4 \hat{k}_J^2}\right)^{1/3} \frac{\epsilon(\hat{R}) - \epsilon(R)}{|V_*''(\hat{R}) - V_+''(\hat{R})|^{1/3}}\,,$$

where μ is the reduced mass of the collision system and

$$\hat{k}_J = \{(2\mu/\hbar^2)[E_{\rm rel} + V_*(\infty) - V_*(\hat{R})]\}^{1/2}\,.$$

The cos τ term stands for the interference between incoming and outgoing partial waves of the autoionizing entrance channel, whereas the Airy expression is a consequence of two points of stationary phase in a nonmonotonic difference potential (for details see ref. [7]). The summation over the heavy particle angular momentum usually smears out the fast oscillations associated with the cos τ term, so that the low energy part of the measured electron spectrum effectively corresponds to an Airy oscillation.

For the argument $z=0$ of the Airy function the electron energy ϵ corresponds to the minimum $\hat{\epsilon}$ of the difference potential; together with

$$\frac{\mathrm{Ai}^2(z_{\max} = -1.018)}{\mathrm{Ai}^2(z=0)} = 0.438 \qquad (4)$$

($\mathrm{Ai}(z_{\max})$ is the maximum of the Airy function) and the knowledge of $V_+(\hat{R})$, the minimum of the entrance channel potential can be determined [6,16]. If the exit channel potential $V_+(R)$ varies slowly around $\hat{R}$, the simple equation

$$\begin{aligned}\Delta V(\infty) - \Delta V(\hat{R}) &\approx \Delta V(\infty) - \Delta V(R_e^*)\\ &= D_e^* + V^+(R_e^*) - V^+(\infty)\,,\end{aligned} \qquad (5)$$

is a good approximation for the entrance channel potential well depth D_e^* (located at R_e^*). For attractive He*+X collision systems (except for X=H), the term $V^+(R_e^*) - V^+(\infty)$ represents only a small correction to D_e^* and can be estimated with almost negligible uncertainty from the ion-induced dipole interaction [1,16].

Extensions of the simple formula (3), including a complete evaluation of the full semiclassical phase shift for a complex potential [21], have been presented [17–21], but for the determination of the well depth for the systems He*($2\,^3$S, $2\,^1$S)+Li, Na, formula (3) in combination with eq. (5) can be considered as sufficiently accurate. We note, however, that angular momentum transfer $|\Delta J| > 0$, discussed in section 3.3, may lead to a non-negligible broadening and shift of the Airy peak in an angle-dependent way, thus limiting to some extent the reliability of the well depth determination on the basis of eqs. (3) and (5).

2.2. Quantum mechanical calculations of electron energy spectra

The quantum theory of Penning and associative ionization has been developed and reviewed by several authors [7,10,11,22–26]. The theoretical derivations are based on a Feshbach projection operator formalism in Born–Oppenheimer approximation. The interaction between the entrance channel of the autoionizing resonance state and the exit channel of the molecular ion and the ejected electron are cast into a nonlocal optical potential for the nuclear motion in the entrance channel.

Assuming a weak electron energy dependence of the coupling, this potential can be approximated by a local one; the radial equation for the entrance channel motion then takes the form

$$\begin{aligned}&\left(-\frac{\hbar^2}{2\mu}\frac{\mathrm{d}^2}{\mathrm{d}R^2} + V_*(R) - \frac{\mathrm{i}}{2}\Gamma(R)\right.\\ &\left.\quad + \frac{\hbar^2}{2\mu}\frac{J_*(J_*+1)}{R^2} - E_*\right) F_*^{J_*}(E_*, R) = 0\,,\end{aligned} \qquad (6)$$

where $\Gamma(R)$ accounts for the loss of the flux in the entrance channel. The corresponding exit channel equation reads

$$\begin{aligned}&\left(-\frac{\hbar^2}{2\mu}\frac{\mathrm{d}^2}{\mathrm{d}R^2} + V_+(R)\right.\\ &\left.\quad + \frac{\hbar^2}{2\mu}\frac{J_+(J_++1)}{R^2} - E_+\right) F_+^{J_+}(E_+, R) = 0\,,\end{aligned} \qquad (7)$$

where E_+ and the real $V_+(R)$ refer to the A+X$^+$ system. Both radial wavefunctions are taken to be energy normalized.

For systems with Σ symmetry the differential cross section with respect to the electron energy is obtained from the radial wavefunctions as [10,23]

$$\begin{aligned}&\frac{\mathrm{d}\sigma}{\mathrm{d}\epsilon}(E_*, E_+)\\ &\quad = g_* \frac{4\pi^3}{k_*^2} \sum_{J_+} \sum_{J_* l} (2J_+ + 1)(2J_* + 1)\\ &\quad \times \begin{pmatrix} J_* & J_+ & l \\ 0 & 0 & 0 \end{pmatrix}^2 \exp(-2\,\mathrm{Im}\,\eta_*^{J_*})\\ &\quad \times |\langle F_+^{J_+}(E_+, R)|\langle \epsilon l|R\rangle|F_*^{J_*}(E_*, R)\rangle|^2\,.\end{aligned} \qquad (8)$$

Here $\eta_*^{J_*}$ is the entrance channel (complex) phase shift, k_* the asymptotic wave vector of the entrance channel motion, and g_* the statistical weight of the autoionizing entrance channel ($g_*=1/3$ for the He*(2 ^{3}S)+H, Li, Na, $g_*=1$ for He*(2 ^{1}S)+Na). Further,

$$\langle \epsilon l | R \rangle = \langle \Psi_{+l}(R, \epsilon) | H_{\mathrm{el}} | \Psi_*(R) \rangle \tag{9}$$

represents the electronic coupling matrix element evaluated in molecule-fixed coordinate system for an ejected electron carrying the angular momentum l with respect to the center of mass. In compliance with the local approximation its energy is given by eq. (1).

The imaginary part of the entrance channel potential is related to these coupling matrix elements by [10]

$$\Gamma(R) = 2\pi \sum_l | \langle \epsilon l | R \rangle |^2 . \tag{10}$$

Lacking information on the individual function $\langle \epsilon l | R \rangle$ from ab initio calculations, one may proceed, as done by Hickman and Morgner [11], by factorizing $\langle \epsilon l | R \rangle$ into a known (or fitted) part $\Gamma^{1/2}(R)$ and functions $\alpha_l(R)$, which are expected to vary slowly as compared to the radial functions. With stationary phase arguments one may even use constants α_l [11], which are suitably chosen (see section 3.3). In this way, model studies incorporating rotational energy changes $\Delta J = J_+ - J_*$ can be carried out and be used – exploiting the interrelation between the electron detection angle, the preferred ΔJ values and the J_* range, which contributes dominantly to certain parts of the spectra – to understand important aspects of the angular dependence of the electron spectra (see section 3.3, fig. 18).

So far, however, the following approximation [11] in the analysis of Penning electron spectra has been commonly used [8–14]

$$\begin{aligned} &\frac{\mathrm{d}\sigma}{\mathrm{d}\epsilon}(E_+, E_*) \\ &\quad = g_* \frac{2\pi^2}{k_*^2} \sum_J (2J+1) \exp(-2\,\mathrm{Im}\, \eta_*^J) \\ &\quad \times | \langle F_+^J(E_+, R) | \Gamma^{1/2}(R) | F_*^J(E_*, R) \rangle |^2 . \end{aligned} \tag{11}$$

The rather simple treatment by eq. (11) does indeed reproduce the main structures of Penning electron spectra, provided that accurate potentials $V_*(R)$, $V_+(R)$ and a reasonable width $\Gamma(R)$ are used. We adopt this approximation for the analysis of our spectra in section 3 (except for the results in fig. 18). The potentials used there are derived from large scale CI calculations, in which the resonance state is defined by a Feshbach projection, based on the occupation pattern of the He-1s shell [15]. The spectra are mostly discussed on the basis of model width functions. Our ab initio width functions used for He*+Li, Na have been obtained by a variant of the Stieltjes imaging procedure, which uses an analytical fit to the step function:

$$I(\epsilon) = \sum_i^{\epsilon_i < \epsilon} | \langle \Psi_+(R, \epsilon_i) | H_{\mathrm{el}} | \Psi_*(R) \rangle |^2 ,$$

constructed from discretized L^2 continuum states $\Psi_+(R, \epsilon_i)$, where [15]

$$\Gamma(R) = 2\pi (\mathrm{d}I/\mathrm{d}\epsilon)|_{\epsilon = E_* - E_+} .$$

It should be noted here that better agreement is obtained when electron energy distributions, calculated on the basis of eq. (11), are compared with spectra measured at $\theta = 90°$ than with angle-integrated experimental spectra [13], since for systems such as He*(2 ^{3}S)+Li, Na the $\Delta J = 0$ approximation, contained in eq. (11), is best fulfilled for angles around 90°. The integrated distributions are usually broader and less structured than the ones calculated with eq. (11). We attribute this in part to the approximations leading from eq. (8) to eq. (11); one important point is the fact that the points of stationary phase are indeed rather different for the integrals involving different J_+ and the same J_*. Rotational excitation or de-excitation during the autoionization process leads to shifts of the electron spectra towards lower and higher energies, respectively.

In connection with our angle-integrating experimental setup (see fig. 6) we point out that the detected angular range extends from $\theta = 35°$ to $\theta = 145°$ with a θ-dependent weighting function (see section 3.2). We also note that the experimental spectra are influenced, although in a minor way, by angle-dependent electron energy shifts due to the Doppler effect, which is associated with the center-of-mass motion of the ionizing collision system.

3. Experimental and theoretical results

3.1. $He^*(2\,^3S)+H(1\,^2S)$

The various experimental and theoretical studies published on the simplest Penning ionization system $He^*(2\,^3S_1)+H(1\,^2S_{1/2})$ have recently been reviewed in the publication of Waibel et al. [9], so here we concentrate on new results. We have reproduced the calculated cross sections and spectra of Waibel et al. [9] with a new, efficient program package developed by one of us (WM) [15]) which has been used for all the computations reported in this paper. The present calculations were carried out with ab initio potential data, obtained recently both for the entrance channel V_* and the exit channel V_+ [15]. The $He^*(2\,^3S)+H(1\,^2S)$ potential differs slightly from the one used earlier [9] at small R; in particular, the well depth D_e^* ($R_e^*=3.4\,a_0$) $=2.284$ eV is now 7 meV deeper than before. The $He(1\,^1S)+H^+$ potential [15] agrees with the one due to Bishop and Cheung [27] and Kolos and Peek [28] to better than 3 meV at all distances reported, but adds further points as required for the collision process under investigation.

In fig. 1 we summarize three electron spectra, calculated with identical input parameters ($V_*(R)$, $V_+(R)$: ref. [15]; $f(E_{rel})$, resolution ΔE: ref. [9]) for different choices of the autoionization width. They are compared with an experimental spectrum for $T_H=300$ K (average collision energy $\bar{E}_{rel}=50$ meV), due to Waibel et al. [9] (note that the structure in the experimental spectrum at energies below 4.5 eV is an artifact associated with the subtraction of contributions due to the ionization of H_2 in the mixed (H, H_2) target). The respective width functions are shown in fig. 2, together with the fit result of ref. [9]. Figs. 1 and 2 serve to illustrate how the shape of the width function influences the electron energy spectrum, as partly discussed earlier [9]. The ab initio width of Hickman et al. [25] is significantly larger for $R>3.5\,a_0$ than the other width functions; this leads to a higher weight for the outer point of stationary phase and therefore to a stronger undulation of the Airy structure, as shown in fig. 1a.

The results for $\Gamma(R)$ due to Morgner and Niehaus [8] as well as our model width have both been adjusted to yield a satisfactory fit to the respective, measured spectra [8,9]. The obvious differences in the calculated spectra mainly reflect the differences between the experimental results of refs. [8,9], which may be, at least in part, associated with uncertainties in the respective transmission functions of the electron spectrometers. The PI to AI ratio in the calculated spectrum fig. 1b is significantly smaller than the experimental one due to Waibel et al. [9]. This is due to the shape of the width proposed by Morgner and Niehaus [8], which switches comparatively softly from the long-range part into saturation, so that the associative part of the spectrum gets a higher weight.

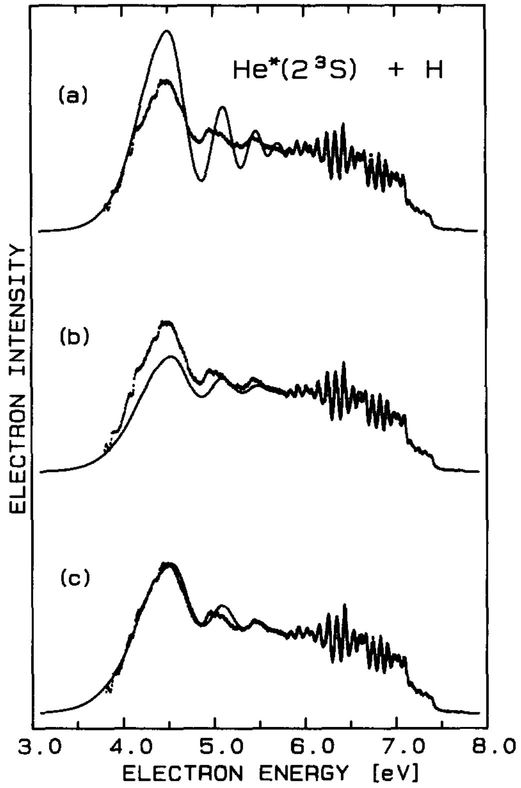

Fig. 1. Comparison of experimental electron energy spectrum for $He^*(2\,^3S)+H(1\,^2S)$ ($\bar{E}_{rel}=50$ meV) [9] with theoretical spectra (smooth lines), calculated on the basis of eq. (11) with ab initio potentials $V_*(R)$, $V_+(R)$ [15] and three different width functions $\Gamma(R)$ (see fig. 2): (a) ab initio width of Hickman et al. [25]; (b) semi-empirically determined width due to Morgner and Niehaus [8]; (c) semi-empirically adjusted width obtained in the present work. The theoretical results contain a convolution with a spectrometer function of 35 meV fwhm.

Our model autoionization width is similar to the one of Waibel et al. [9]. It differs slightly for $R<3$

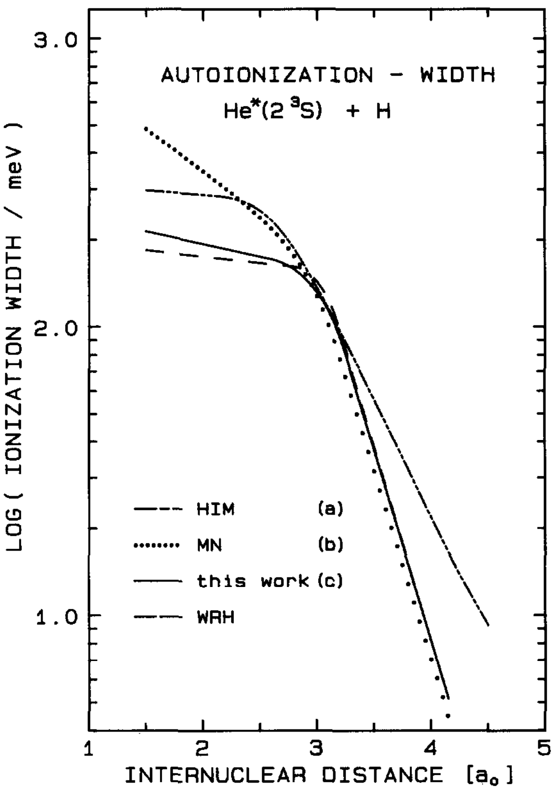

Fig. 2. Autoionization width functions $\Gamma(R)$ for $He^*(2\,^3S)+H(1\,^2S)$, as given previously ((a) HIM: ab initio calculation [25]; (b) MN: semi-empirical fit [8]; WRH: semi-empirical fit [9]) and determined in the present work (c) by fitting the experimental spectrum, reported in ref. [9] ($\bar{E}_{rel}=50$ meV).

a_0, which is in part a consequence of the new potential data. A detailed comparison between the theoretical spectrum (c), the one calculated by Waibel et al. [9] and the experimental results [9] shows the current improvement, which leads to almost optimal agreement within the given model.

An interesting result of our model calculations is the fact that the associative part of the spectrum with the complex rovibrational structure is almost independent of the shape of $\Gamma(R)$, whereas the Penning part of the spectrum is substantially more sensitive to $\Gamma(R)$. The ratio of both is also an important property for the semi-empirical determination of the width function.

The energy-dependent total ionization cross sections, resulting from the four different versions of $\Gamma(R)$ agree within 10%, although the corresponding electron energy spectra are quite different in shape. This demonstrates that the published experimental results for the total ionization cross sections [8,29,30] with their typical uncertainties of 20–30% are not sufficiently accurate to provide a significant test of the width function (see also the discussion in ref. [9]).

Besides the important influence of the width function $\Gamma(R)$ on the electron spectrum, we would like to address here the dependence on collision energy (clearly the shapes of the potentials $V_*(r)$ and $V_+(R)$ are also important, but their influence has been discussed before in detail [8,9]). For attractive Penning systems ($E_{rel} \ll D_e^*$), the collision energy dependence of the cross sections is mainly due to the variation of the number of heavy particle partial waves, which effectively contribute to ionization by surmounting the rotational barrier ($0 \leqslant J_* \leqslant J_c(E_{rel})$) and accessing short distances with a large width [9,31]. As long as E_{rel} is sufficiently small ($E_{rel}/D_e^* \lesssim 0.3$), the opacities O_J are nearly constant $O_J \approx \bar{O}$ for all $J \leqslant J_c$ and close to zero otherwise. Therefore the general expression for the total ionization cross section

$$\sigma_{TI} = (g_* \pi \hbar^2 / 2\mu E_{rel}) \sum_{J=0}^{\infty} (2J+1) O_J(E_{rel}) , \qquad (12)$$

simplifies to

$$\sigma_{TI} \approx (g_* \pi \hbar^2 / 2\mu E_{rel}) (J_c+1)^2 \bar{O} . \qquad (13)$$

Eq. (13) expresses the essential dependence of the total ionization cross sections on $J_c(E_{rel})$. J_c depends critically on the behaviour of $V_*(R)$ at larger distances [31] (for $He^*(2\,^3S)+H$: $8 \lesssim R \lesssim 15\ a_0$ [9]); therefore it is important to have potentials $V_*(R)$ available, which are reliable in the R range, where the rotational barrier is located (see also the discussion for He* + Na).

In fig. 3 we present electron spectra for $He^*(2\,^3S)+H$, calculated at six discrete collision energies between 1 and 370 meV; the width function (c) (fig. 2) was used to obtain these results and those in figs. 4 and 5. The variation of the spectral shapes is mainly due to the E_{rel} dependence of J_c (which are listed in fig. 3). At $E_{rel}=1$ meV, the Penning part of the spectrum ($\epsilon < E_0 = 6.22$ eV) essentially corresponds to a modified sinus oscillation, as observed

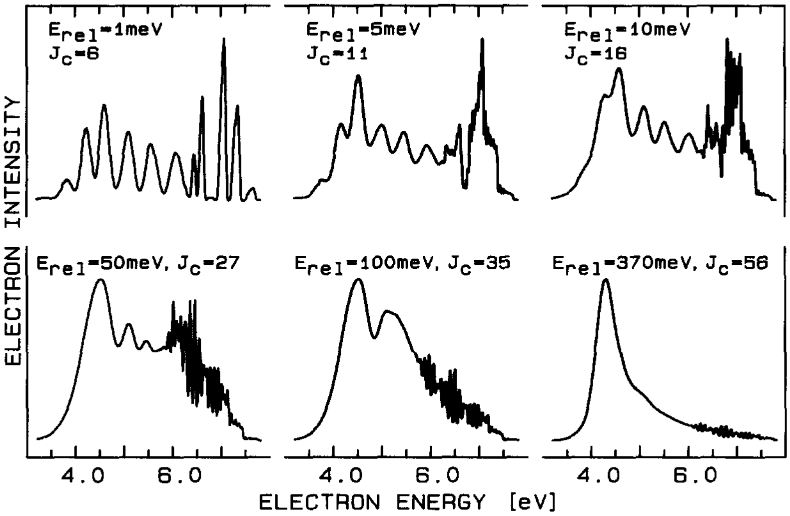

Fig. 3. Collision energy dependence of the theoretical electron spectra for $He^*(2\,^3S)+H(1\,^2S)$, as calculated for six discrete collision energies E_{rel} on the basis of eq. (11) with ab initio potentials $V_*(R)$, $V_+(R)$ [15] and the width $\Gamma(R)$ determined in the present work (see fig. 2c). The respective J_c corresponds to the maximum orbital angular momentum, associated with "close collisions" (see text).

for any partial electron spectrum, calculated for a single J value and not too strong Γ. These oscillations are due to both in–out interferences of the heavy particle motion in the entrance channel (leading to the so-called "fast" or "rapid" oscillations) and entrance–exit channel interferences (Airy structure).

In fig. 4, we show for illustration partial electron spectra calculated for $E_{rel}=50$ meV at seven different J values. The vertical lines indicate the positions of the main and first supernumerary Airy peak of the full spectrum, shown in fig. 3. The overall smooth Airy structure results in an intricate way through the summation of the different partial J spectra, in which the locations of the peaks in the "fast oscillations" vary with J. We note that those features have also been discussed in the context of optical bound–free transitions, and we refer the reader to the interesting review paper by Tellinghuisen [32].

The AI part of the spectrum at energies $\epsilon \gtrsim 6.2$ eV (formation of HeH^+ ions) is strongly dependent on J, as has been analyzed in detail by Waibel et al. [9]. With rising J, the classical turning point in the entrance channel potential moves towards larger internuclear distances. This change results in a decrease of the electron energy $\epsilon(R)$ in the region of favourable Franck–Condon overlap, so that higher electron energies disappear with increasing J. Expressed in a different way, this behaviour is due to the progressive loss of vibrationally bound states with rising J.

In fig. 5 we show the correlation between the shape of the electron spectrum and the number of contributing angular momenta J_* for the discrete collision energy $E_{rel}=50$ meV. The value of J is stepwise increased by 5 units from $J=5$ to $J=25$ with $J_c=27$ being the maximum partial wave with a large opacity ($\bar{O}\approx 0.83$). The shape of the spectrum for $J=0$–5 is practically identical with the full spectrum for $E_{rel}=1$ meV in fig. 3, and the spectrum for the range $J=0$–10 is similar to the full one for $E_{rel}=5$ meV in accordance with the J_c values listed in fig. 3. The main Airy peak appears within the first fifteen partial waves; it looses its additional "fast" oscillatory structure only after the highest partial waves are taken into account. So far fast oscillations have not been clearly observed in experiments on $He^*(2\,^3S)+H$. With their cooled H and He* beams, Waibel et al. [9] could have detected them, but they restricted their study to the AI part of the spectrum. Fig. 5 shows that the width of the main Airy peak comprises about three "fast" oscillations, whereas the distances of the first and second supernumerary Airy peaks in the full spectrum correspond to a single fast oscillation only. The posi-

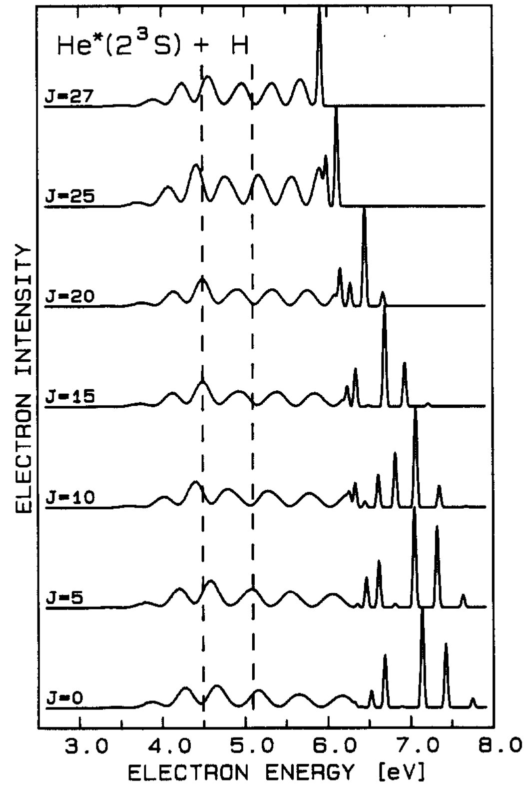

Fig. 4. J-dependent partial electron spectra for $He^*(2\,^3S)+H(1\,^2S)$, calculated at the discrete collision energy $E_{rel}=50$ meV with input data described in the caption for fig. 3.

tions of these peaks shift noticeably, when $J=26$, 27 contributions are added; this is relevant for a proper comparison of experimental and theoretical data, especially if velocity-selected atomic beams were used in future work.

The associative part of the spectrum has been measured with two different collision energy distributions and analyzed in detail [9], so we do not dwell on AI further. Good agreement between experiment and the calculated AI spectra is observed, but we note again (see also fig. 1) that the shape of the AI spectrum is – for given $V_*(R)$, $V_+(R)$ and collision energy distribution – rather insensitive to the choice of the width function.

In conclusion of this section, we stress that all these calculations and statements are made using eq. (11), i.e. assuming that the angular momentum of the heavy particles is conserved upon electron emission. Based on a classical estimate [13], the angular momentum change due to the recoil effect of an electron emitted from He* should in fact include at most $|\Delta J|=1$ transitions for $He^*(2\,^3S)+H$, but the Coulomb interaction between the ion and the emitted electron may lead to considerably larger $|\Delta J|$. One should also note here that the comparison is made between an angle-integrated theoretical spectrum and an experimental one taken for a certain angular range. Thus, the shape of the fitted $\Gamma(R)$ may be an artifact of this inadequate theoretical treatment. Indeed, our recent preliminary ab initio results for the width [14] are not compatible with the semi-empirically fitted forms (see fig. 2 and refs. [8,9]), but similar in shape to the ab initio results of Hickman et al. [25] (see fig. 2a). Clearly, more experimental and theoretical work is needed. In this connection, we plan to measure the angular dependence of the electron spectrum for $He^*(2\,^3S)+H$, not studied so far.

3.2. $He(2\,^3S,\,2\,^1S)+Na(3\,^2S)$

In this and the following sections we present new experimental results. Fig. 6 shows schematically the crossed beam setup used, including the cylindrical mirror analyzer (CMA) [12,13], the metastable atom source [16], and the metal vapour oven [16], as used for the lithium measurements; the results for sodium were obtained with a two-chamber oven supplied by Meijer [33]. The CMA was operated at a constant transmission energy of 8 eV, and the effective energy resolution was determined as 40–50 meV (fwhm) through a peak shape analysis of simultaneously recorded $He^*(2\,^1S,\,2\,^3S)+NO$ spectra. In addition the NO gas was useful for stabilizing the surface potentials [34], which otherwise changed by as much as 50 meV/h because of the alkali beams. The insert in fig. 6 shows the entrance slit part of the CMA in relation to the atomic beam directions, including the relevant angles for electron detection.

Fig. 7a presents the $He^*(2\,^3S,\,2\,^1S)+Na$ electron energy spectra recorded with $\Delta\varphi=2\pi$ corresponding to an acceptance range of $35° \leqslant \theta \leqslant 145°$ of the spectrometer, i.e. integration over a wide range of the electron emission angle relative to $v_{rel}=v_{He}-v_{Na}$. The shapes of the spectra are quite similar to those of the angle-integrated data published for He*+Li [13]. In particular the minimum between the main Airy peak

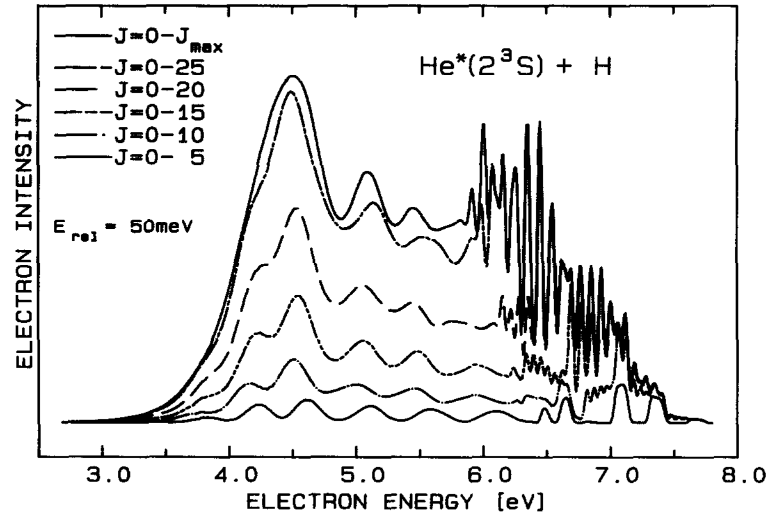

Fig. 5. Evolution of the electron spectrum for He*(2 ^{3}S)+H(1 ^{2}S) with increasing number of contributing angular momenta J, as calculated for $E_{rel} = 50$ meV (see also caption for fig. 3).

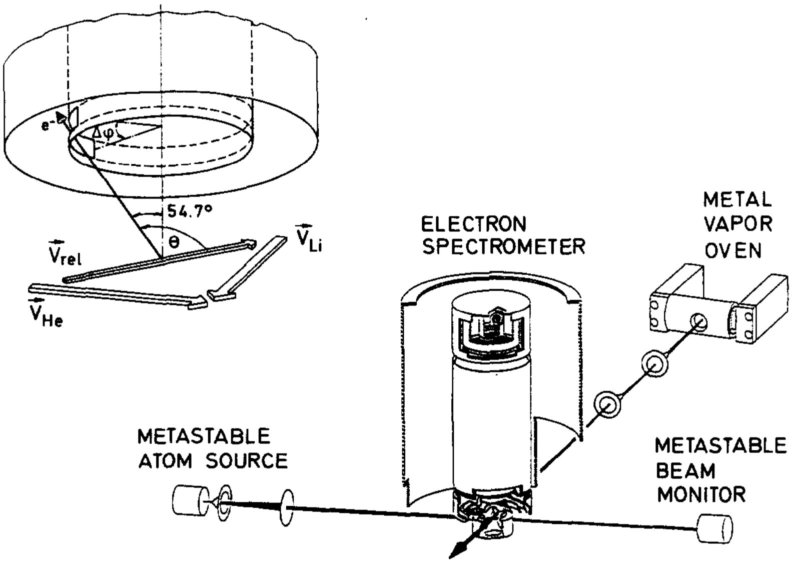

Fig. 6. Semi-schematic drawing of the crossed beam apparatus used to study the electron energy spectra for the systems He*(2 ^{3}S, 2 ^{1}S)+Li, Na. The insert illustrates the method to measure spectra for different electron ejection angles θ (with respect to the relative velocity vector $v_{rel} = v_{He^*} - v_X$) by using selected ranges $\Delta\varphi$ of the cylindrical mirror analyzer.

and the first supernumerary peak is washed out in the He*(2 ^{3}S)+Na part of the spectrum as seen before for He*(2 ^{3}S)+Li. Note that in the present experimental setup "integrated" electron spectra contain a φ-integration over 2π, which corresponds to a θ-integration over the range $35° \leqslant \theta \leqslant 145°$ according to $\cos\theta = \sin\vartheta \cos\varphi$ ($\vartheta = 55° \pm 3°$). When comparing experimentally integrated spectra with angle-inte-

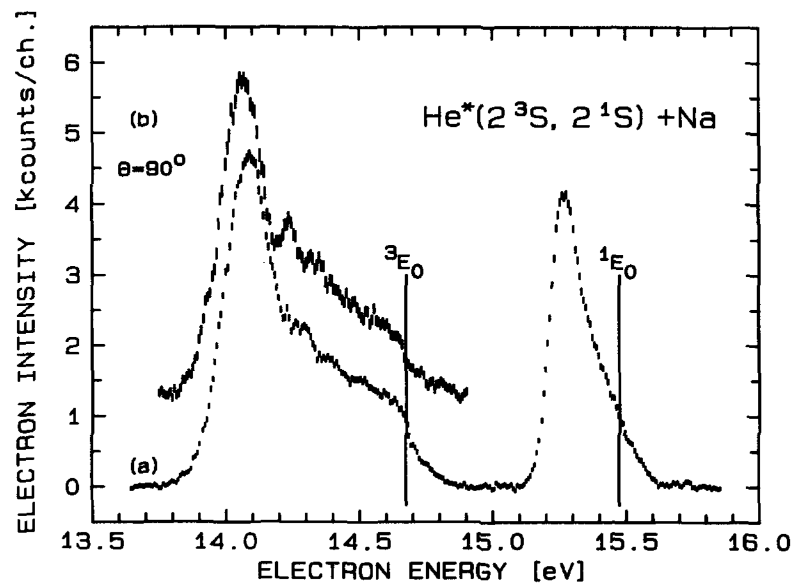

Fig. 7. Electron energy spectra for He*(2 ^{3}S, 2 ^{1}S) + Na using the apparatus shown in fig. 6 with full azimuthal range $\Delta\varphi \approx 2\pi$ (data set (a)); for comparison, the data (b) show a He*(2 ^{3}S) + Na spectrum, obtained with a selected $\Delta\varphi$ range, corresponding to $\theta \approx (90 \pm 25)°$. The average collision energy was $\bar{E}_{rel} = 70$ meV. The vertical lines, labelled $^3E_0$ and $^1E_0$, denote the asymptotic energy differences ("nominal energies") of the respective difference potentials for He*(2 ^{3}S) + Na and He*(2 ^{1}S) + Na.

grated theoretical cross sections, a θ-dependent weighting function has to be considered

$$\frac{d\sigma^{\text{exp}}}{d\epsilon} \sim \int_{35^\circ}^{145^\circ} \frac{\sin\theta}{\sqrt{\sin^2\vartheta - \cos^2\theta}} \frac{d\sigma(\theta, \epsilon)}{d\theta\, d\epsilon}\, d\theta . \qquad (14)$$

Therefore, the "forward" ($\theta = 45° \pm 10°$) and the "backward" ($\theta = 135° \pm 10°$) directions get a higher weight in the experimental integration procedure.

Proceeding in the same way as for He* + Li [13], we have reduced the acceptance range for electron detection to a limited $\Delta\varphi$ section. The He*(2 ^{3}S) + Na spectrum, labelled $\theta = 90°$ in fig. 7b, was recorded for $\theta = 90° \pm 25°$ with $\Delta\varphi \approx 70°$ ($\cos\theta = \sin\vartheta \cos\varphi$, $\vartheta = 55° \pm 3°$). Although the statistical accuracy is not very good, a somewhat narrower main Airy peak, as well as a minimum between the main and the first supernumerary peak are clearly observed. The maximum of the main peak is shifted by about 30 meV towards lower electron energies compared to the one of the angle-integrated spectrum for reasons discussed later for the similar case He*(2 ^{3}S) + Li. In view of the low count rate (≈ 10 counts/s), we restricted the sodium measurements to the triplet spectrum for $\theta = 90°$, but we plan to extend the study to further electron emission angles with a different experimental setup, that will allow us to include the forward ($\theta = 0°$) and backward ($\theta = 180°$) direction, which is impossible for the geometry of the CMA.

In table 1 the values for the entrance channel potential well depths D_e^* are summarized; the experi-

Table 1
Well depths D_e^* for the systems He*(2 ^{3}S, 2 ^{1}S) + Na(3 ^{2}S) $^2\Sigma$

	D_e^* (meV)	
	a)	b)
experiments:		
$35° \leq \theta \leq 145°$	722 (20)	274 (20)
$\theta = 90(25)°$	726 (20)	-
$\theta = 90°$ [16]	740 (25)	277 (24)
$\theta \approx 90°$ [1]	735 (50)	300 (50)
ab initio calc. [15]	688	250

[a] He*(2 ^{3}S) + Na(3 ^{2}S) $^2\Sigma$.
[b] He*(2 ^{1}S) + Na(3 ^{2}S) $^2\Sigma$.

mental values were determined from an analysis of the low energy edge position of the main Airy peak. Satisfactory overall agreement among the experimental data and between the theoretical ab initio value [15] and the experimental results is observed, but one notes a tendency that all the experimental results are somewhat larger than the ab initio value for D_e^*. This is in line with the fact that the ab initio potentials are obtained variationally; it is estimated that the remaining deficiency in electron correlation may account for about 15 meV of missing attraction [15].

Although the various experimentally determined well depths are in good agreement, we should mention significant differences between the shapes of the three $\theta = 90°$ spectra, obtained so far. They are illustrated in fig. 8, where the data of Hotop and Niehaus [1], of Ruf et al. [16], and of the present work are compared. The experimental conditions regarding the projectile and target beams were almost identical in the later two studies (average collision energy 70 meV), whereas Hotop and Niehaus used an electron beam excited metastable He beam of unmeasured velocity distribution and a static Na target at a temperature around 200°C (estimated average collision energy 50 meV). A distinct discrepancy between the data of Ruf et al. [16] and those of the present work is observed; we attribute this discrepancy mainly to a tricky experimental artifact, which influenced the Na data of Ruf et al. [16] such that the overall detection efficiency of their electron spectrometer was count rate dependent due to a fatigue effect of the channel multiplier. As far as we know, only the shapes of their Na spectra [16] were significantly modified by this effect. For comparison with theoretical calculations, the present spectra should be used. Unfortunately, Padial et al. [14] compared their computed spectra with the data of Ruf et al. [16] at a time, when we had not yet clarified the experimental situation.

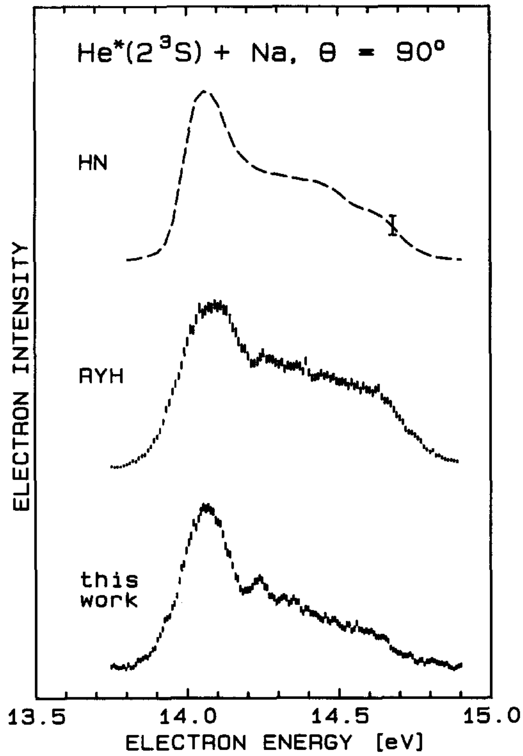

Fig. 8. Comparison of the three available experimental electron spectra for the collision system He*($2\,^3S$)+Na, observed at an average detection angle $\theta = 90°$. HN: Hotop and Niehaus [1], average collision energy $\bar{E}_{rel} \approx 50$ meV; RYH: Ruf et al. [16], $\bar{E}_{rel} = 71$ meV; for the present experiment, $\bar{E}_{rel} = 70$ meV.

For model calculations of the electron spectra two sets of potential curves $V_*(R)$ for He*($2\,^3S$, $2\,^1S$)+Na are available [15,35]. They are shown in fig. 9. Cohen et al. [35] constructed their potentials from (poor) ab initio data, a van der Waals correction and the restraint that the empirical well depths D_e^* [1] should be met. The procedure resulted in potentials (denoted CML and also used by Padial et al. [14]), which are somewhat deeper than the ab initio curves, labelled MM in fig. 9. The respective shapes of the potentials are very different in the attractive, long-range part, especially in the triplet case between $R = 7\ a_0$ and $R = 12\ a_0$. This difference, in fact, influences the calculated electron spectra substantially through the slope of the electron energy function $\epsilon(R)$, the radial wave vector $k_*^J(R)$, and the number of contributing partial waves, which is closely related to the long-range behaviour of the potential curves $V_*(R)$. A quantum mechanical calculation for He*($2\,^3S$)+Na at $E_{rel} = 70$ meV (average collision energy of the present experiment), for example, using the MM potential $V_*(R)$ contains significant partial wave contributions up to $J_* = 84$, whereas with the CML potential only 76 angular momenta contribute.

Using the width function $\Gamma(R)$ computed by Cohen et al. [35] and also used by Padial et al. [14], we

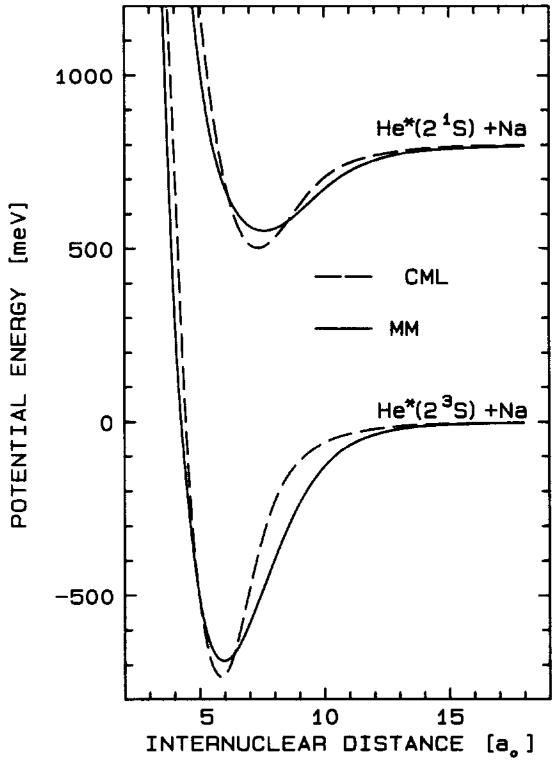

Fig. 9. Comparison of the two sets of potential energy curves available for He*(2 ^{3}S)+Na(3 ^{2}S) $^2\Sigma$ and He*(2 ^{1}S)+Na(3 ^{2}S) $^2\Sigma$. CML: semi-empirical potentials of Cohen et al. [35]; MM: ab initio potentials of the present work (see also ref. [15]).

have calculated electron spectra for He*(2 ^{3}S, 2 ^{1}S)+Na at $E_{\mathrm{rel}}=70$ meV with the two different sets of potentials $V_*(R)$; distinct differences between these two spectra are observed (see fig. 10), both in the shapes and the total cross sections. We note that analogous calculations for He*(2 ^{3}S)+Na, using our preliminary ab initio width $\Gamma(R)$ [15], yield spectra very similar in shape to those obtained with the CML width [35]. The present experimental electron spectrum for He*(2 ^{3}S)+Na at $\theta=90°$ is in significantly better overall agreement with the calculated spectrum based on the MM potential $V_*(R)$ [15] than with the one computed with the CML potential [35], independent of the choice of either width.

In fig. 11 the change of the He*(2 ^{3}S)+Na electron spectrum with collision energy, ranging from 1 to 250 meV, is illustrated. The trends are similar to those observed for the Penning part of the He*(2 ^{3}S)+H spectra (due to the only weakly attractive He+Na$^+$ potential AI is a negligible process for He*+Na) and governed by the number of contributing angular momenta J. Fast oscillations are only visible at $E_{\mathrm{rel}}=1$ meV (all the spectra have been convoluted with a resolution of 50 meV (fwhm)). The peak close to $E_0=14.68$ eV, which comes out prominently at low collision energies only, is due to ionization at larger R, as discussed previously by Padial et al. [14]; they presented "partial" electron spectra, obtained by integrating the transition matrix element over restricted R intervals. We note that with the CML potential $V_*(R)$ [35], which is flatter at larger R than the MM potential [15], a prominent shoulder near E_0 is still present at collision energies as high as 70 meV (see fig. 10).

In fig. 12, we compare calculated He*(2 ^{3}S)+Na spectra (again convoluted with 50 meV spectrometer width) for (a) the collision energy distribution of the present experiment ($\bar{E}_{\mathrm{rel}}=70$ meV), (b) a parallel beam setup involving the same velocity distributions used in (a) ($\bar{E}_{\mathrm{rel}}=20$ meV), and (c) a collision energy distribution for a planned single beam experiment of collinear supersonic He* and Na beams. Spectrum (a) is very similar to the spectrum for the discrete collision energy $E_{\mathrm{rel}}=70$ meV, included in fig. 11; the effect of the collision energy averaging is almost negligible. Spectrum (b) serves to illustrate the connection between a crossed beams and single beam situation. If the beams, crossed in configuration (a) at right angles, collide at a small angle ("parallel beams"), the average collision energy is reduced by a factor of 3.5; this decrease brings out the Airy structure more clearly and leads to a general rise of the high energy part of the spectrum. Interesting additional structures would appear in a single beam experiment, involving equal He* and Na velocity distributions and corresponding to the realization of an average collision energy of about 2 meV.

In conclusion of this section, we discuss the cross section ratio q_s/q_t(Na) for ionization in the systems He*(2 ^{1}S)+Na (q_s) and He*(2 ^{3}S)+Na (q_t) at collision energies around 70 meV (q_s/q_t is only weakly dependent on E_{rel}). Hotop and Niehaus [1] obtained $q_s/q_t(\mathrm{Na})\approx1.2\pm0.1$, calibrating their He*(2 ^{1}S)/He*(2 ^{3}S) flux ratio j_s/j_t with regard to Xe, for which $q_s/q_t(\mathrm{Xe})=1.2$ was assumed. As is now known [16], the latter ratio is in fact much larger,

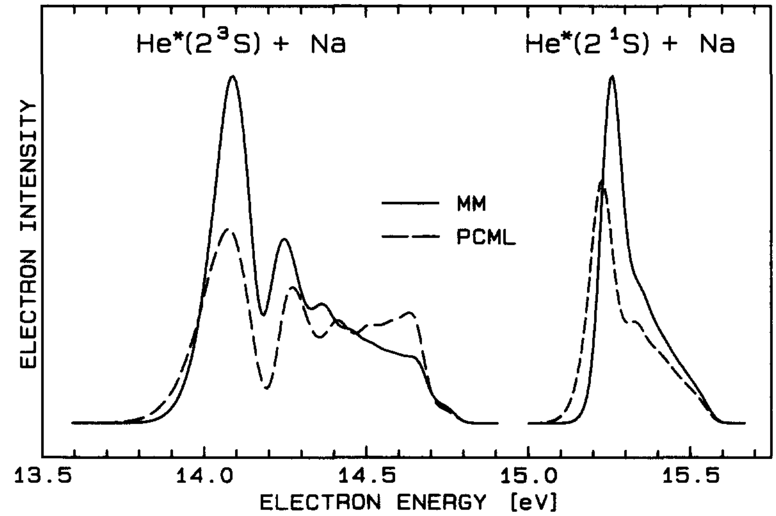

Fig. 10. Comparison of electron energy spectra for the systems He*(2 ^{3}S) + Na(3 ^{2}S) and He*(2 ^{1}S) + Na(3 ^{2}S), calculated for the discrete collision energy $E_{rel} = 70$ meV with the two different sets of entrance channel potentials $V_*(R)$ shown in fig. 9, with our ab initio potential $V_+(R)$ [15], and with the width functions of Cohen et al. [35]. MM: $V_*(R)$ of the present work (see also ref. [15]); PCML: $V_*(R)$ due to Cohen et al. [35] and used previously in calculations of the electron spectra by Padial et al. [14]. The spectra are convoluted with a spectrometer function of 50 meV fwhm. The intensity scale of the two spectra for the same system is, respectively, identical, but different for 2 ^{3}S and 2 ^{1}S. The corresponding total ionization cross sections for He*(2 ^{3}S) + Na (q_t) and for He*(2 ^{1}S) + Na (q_s) in units 10^{-20} m^2 are as follows: q_t: 39.6 (MM), 32.2 (PCML); q_s: 85.0 (MM), 70.2 (PCML).

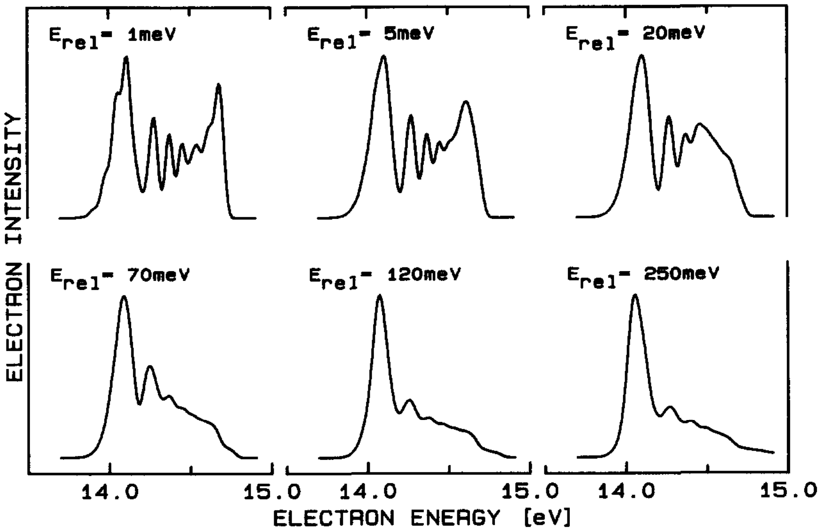

Fig. 11. Collision energy dependence of the electron spectra for He*(2 ^{3}S) + Na, as calculated for six discrete collision energies E_{rel} on the basis of eq. (11) with our ab initio potentials $V_*(R)$ and $V_+(R)$ (fig. 9 and ref. [15]) and the width of Meyer and Movre [15]. The spectra are convoluted with a spectrometer function of 50 meV fwhm. The respective total ionization cross sections q_t (10^{-20} m^2) are in order of rising E_{rel}: 181.7, 118.5, 71.7, 48.0, 42.0, 27.5.

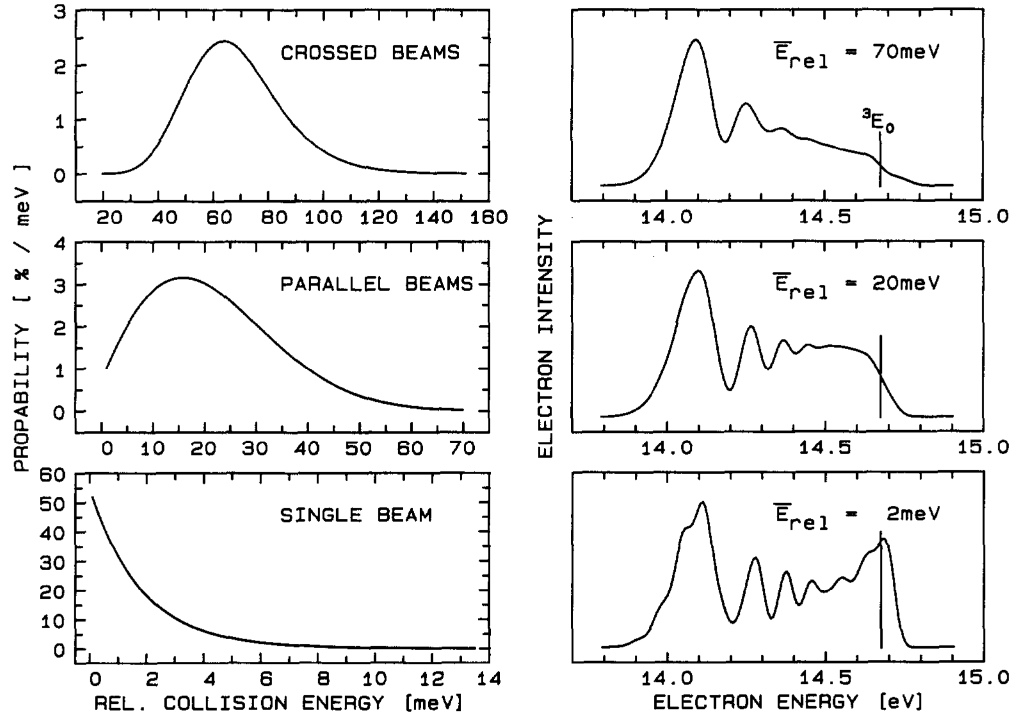

Fig. 12. Electron energy spectra for He*(2 ^{3}S)+Na, calculated with the ab initio potentials and width [15] for different collision energy distributions.

but it is not possible to accurately re-evaluate the old data [1] in view of uncertainties in the He* velocity distribution. Ruf et al. [16] determined $q_s/q_t(\mathrm{Na})=3.1\pm30\%$; it is difficult to judge to what extent their ratio q_s/q_t was affected by the detector problem mentioned above, but we note that their measured ratios q_s/q_t for all alkali atoms Li to Cs were in the range 3.1–4.0. From our angle-integrated spectra (see fig. 7) and determination of j_s/j_t by means of the Xe spectra [16] we obtain $q_s/q_t(\mathrm{Na})=2.8\pm30\%$. Note that the given uncertainty is mainly associated with the error limit attached to $q_s/q_t(\mathrm{Xe})$ (see ref. [16]).

Cohen et al. [35] obtained a calculated cross section ratio of 2.2, using their semi-empirical potentials and their ab initio width to compute total ionization cross sections. We have reproduced this result and obtain $q_s/q_t(\mathrm{Na})=2.18$ at $E_{rel}=70$ meV. Using the MM potentials $V_*(R)$ and the CML width, we calculate $q_s/q_t(\mathrm{Na})=2.15$ at $E_{rel}=70$ meV. These calculated cross section ratios are distinctly smaller than 3, which is the ratio g_{*s}/g_{*t} of the statistical weights for spin-allowed collisions in the two systems. This result is due to the fact that the calculated opacities are distinctly smaller for He*(2 ^{1}S)+Na than for He*(2 ^{3}S)+Na, overriding the opposite effect that the long-range close collision cross section is somewhat larger for He*(2 ^{1}S)+Na. The present experimental uncertainties unfortunately do not allow a sensitive test of the theoretical ratio q_s/q_t.

3.3. He*(2 ^{3}S)+Li

The calculations described in sections 3.1 and 3.2 have demonstrated some of the important dependences of the electron spectra for attractive Penning ionization systems, namely on the potentials $V_*(R)$ (fig. 10), on the width function $\Gamma(R)$ (fig. 1), and on collision energy as well as the number of contributing heavy particle waves. The system He*(2 ^{3}S)+Li is similar to He*(2 ^{3}S)+Na; it has been studied by ion spectrometry [36] and in detail by electron spectrometry [13]; the clearly observed, angular-dependent Airy structure in the electron spectrum [13] provides a sensitive test of the theory.

We start the discussion of this system with an investigation of the dependence of the electron spectrum on the width function $\Gamma(R)$, which we carried out before any ab initio width [13,15] was available. It is demonstrated that nearly identical spectra can be obtained with very different width functions and that only experimental data with sufficiently high resolution and statistical quality may discriminate between them. Thus, reliable theoretical width functions are of crucial importance. In connection with the necessity to include $\Delta J \neq 0$ transitions, it is clear that fit calculations of the electron spectra on the basis of the $\Delta J=0$ approximation may only serve as a guide.

In fig. 13, we summarize three model widths Γ_1, Γ_2, Γ_3 together with the ab initio width Γ_{MM} [15], which turned out to be rather close to the choice Γ_3. With the accurate ab initio potentials $V_*(R)$ and $V_+(R)$ [13], the various widths yield absolute ionization cross sections (see table 2), which are all compatible with the experimental value [36] within the stated uncertainty of ± 30%. Note that the measurement [36] was carried out with a metastable He* beam, which contained some He*($2\,^1S$) besides the dominant He*($2\,^3S$) component; this He*($2\,^1S$) contribution results in an average cross section higher than the true He*($2\,^3S$) cross section (the singlet to triplet cross section ratio is $q_s/q_t \approx 3.5$ [13,16]). Incidentally, the He*($2\,^1S$) contribution may also – at least in part – account for the low value of the well depth $D_e^* \approx 0.7$ eV for He*($2\,^3S$)+Li, estimated in ref. [36] from the kinetic energy spectrum of the Li^+ ions. The opacities O_J come out very close to 1 for the widths Γ_1, Γ_2, whereas for Γ_3 and Γ_{MM}, they are about 0.8 and 0.73, respectively. With these large values for O_J it is clear – within the close collision model (see section 3.1) – that the absolute cross section is insensitive to $\Gamma(R)$.

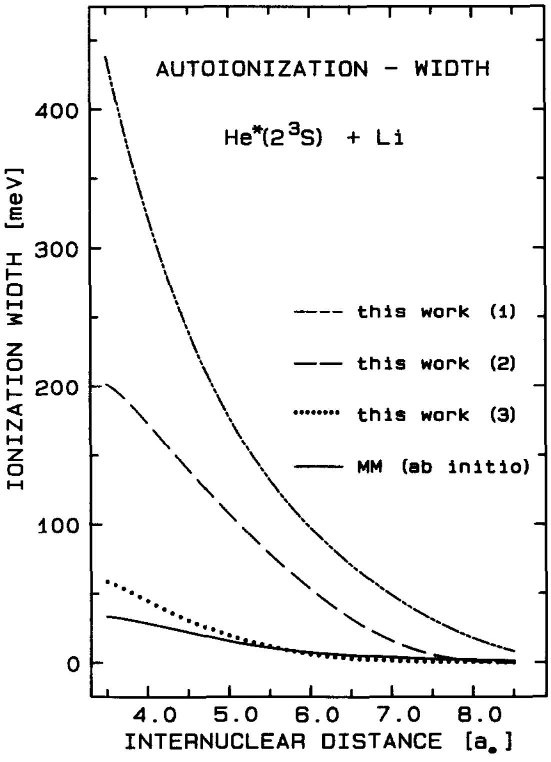

Fig. 13. Autoionization width functions $\Gamma(R)$ used in the different calculations of the electron energy spectrum for He*($2\,^3S$)+Li($2\,^2S$), shown in fig. 14.

In fig. 14a we compare the electron spectra, calculated with the model widths, and the experimental spectrum, measured at $\theta = 90°$ [16]; the spectra have been normalized at the main Airy peak. Surprisingly, the spectral shapes computed with Γ_1 and Γ_3 are very similar and both in good agreement with experiment except at energies $\epsilon > E_0$, where only the smaller width Γ_3 leads to a sizeable cross section. The choice Γ_2 leads to a prominent main Airy peak, but, relatively, to much too small cross sections in the other regions of the spectrum. Both Γ_1 and Γ_2 lead to full saturation ($O_J = 1$) for $J \leqslant J_c$ such that essentially no flux penetrates to the repulsive wall region; consequently, no electron intensity with $\epsilon > E_0$ is observed. In contrast saturation effects are sufficiently reduced for Γ_3 ($O_J \approx 0.8$) so that – as is also seen in the experimental results – a high energy tail develops. In fig. 14b, the experimental data [16] are compared with the fully ab initio calculated spectrum; the adopted intensity normalization around 14.2 eV leads to very good agreement in the range 13.9–14.6 eV, but the experimental main Airy peak is lower and broader than the calculated one. As far as we know at this time (also by comparison with the more recent $\theta = 90°$ data [13]), the He*+Li results of Ruf et al. [16] were not significantly affected by the detector problem,

Table 2
Total ionization cross sections σ_{TI} (10^{-20} m^2) for He*(2 ^{3}S) + Li(2 ^{2}S) calculated with ab initio width Γ_{MM} and model widths Γ_1–Γ_3

E_{rel} (meV)	Quantum mechanical calculations [a]				Experiment [b]
	Γ_{MM}	Γ_1	Γ_2	Γ_3	
20	62.3	86.7	86.5	67.3	92
40	55.3	73.2	73.2	59.1	72
60	46.8	63.7	63.6	49.0	63
80	43.6	59.9	59.8	46.0	57
100	40.8	56.7	56.5	42.8	53
140	35.5	50.9	50.5	36.8	47
180	32.6	47.5	46.9	33.3	43
220	30.1	45.1	44.4	30.4	41
260	28.7	43.8	43.2	28.3	38
300	26.4	41.0	40.3	25.9	36
340	24.4	38.0	37.5	23.8	35

[a] The respective width functions $\Gamma(R)$ are shown in fig. 13.

[b] Merged-beams experiment [36] with typical uncertainty of ± 30% for the absolute cross section scale; note that the He* beam contained a minor fraction of He*(2 ^{1}S). The listed numbers were read from fig. 5 in ref. [36].

which influenced their He* + Na data (see section 3.2). On the other hand, ΔJ transfer may, in fact, lead to a broadened and shifted Airy peak structure (see below).

Fig. 15 shows the J composition of the electron spectrum for He*(2 ^{3}S) + Li at $E_{rel} = 100$ meV; the ab initio width and potentials [13,15] have been used for the calculations (fig. 15 may also serve to describe the corresponding behaviour for the similar collision system He*(2 ^{3}S) + Na). The only contributions to the weak process of associative ionization ($\epsilon > E_0 + E_{rel} = 14.53$ eV) are due to small angular momenta ($J < 20$). The highest ten partial waves ($J = 71$–$J_{max} = 80$) contribute strongly to the main Airy peak, but very little to the first supernumerary peak. The partial waves $J = 41$–60 contribute strongly to both the main and the first two supernumerary Airy peaks, and the waves $J = 61$–70 influence the main and the first supernumerary Airy peak (see also fig. 5 in ref. [13]); these facts are important for the discussion of the angular dependence of the electron spectra.

In order to illustrate the collision energy dependence of the electron energy distribution for He*(2 ^{3}S) + Li, we present in fig. 16 four spectra, calculated at discrete collision energies between 10 and 300 meV with the ab initio width and potentials. The behaviour is analogous to the similar case He*(2 ^{3}S) + Na (see fig. 11). In order to observe rapid oscillations, collision energies below 10 meV have to be realized.

Taking up our previous discussion of the substantial angular dependence of the electron energy spectrum for attractive Penning ionization systems [13] we present in fig. 17 five electron spectra measured for He*(2 ^{3}S) + Li at different detection angles. The spectral shapes change clearly with the electron emission angle θ (referred to the relative velocity $v_{rel} = v_{He} - v_{Li}$), especially the positions of the main and supernumerary peaks shift continuously from $\theta = 45°$ to $135°$. This dependence of the electron energy spectrum on the detection angle is a consequence of angular momentum transfer ($\Delta J \neq 0$).

As discussed previously [13], the observed θ-dependent shifts can be qualitatively explained by preferential transfers with $\Delta J < 0$ in forward direction, with $\Delta J > 0$ in backward direction, but both signs of ΔJ occur at $\theta = 90°$. Classical trajectory calculations show (fig. 5, ref. [13]) that for most of the contributing partial waves J_* the orientation of the axis of the heavy particle system in the center-of-mass frame covers only a fairly small angular range for distances, where most of the ionizing transitions occur. The electron spectrum is influenced in a non-uniform way, since, on the one hand, different groups of angular momenta dominate different parts of the electron energy spectrum (see fig. 15) and, on the other hand, directed angular momentum transfer ($\Delta J < 0$ or

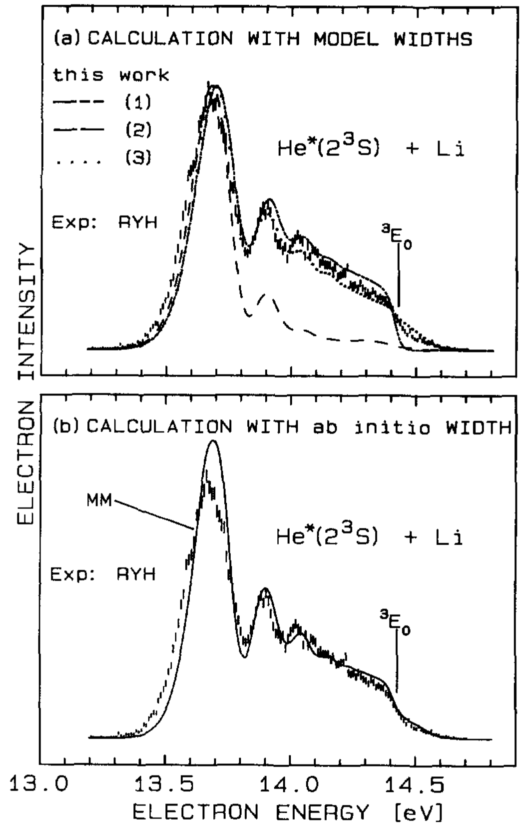

Fig. 14. Comparison of experimental electron energy spectrum for He*(2 ^{3}S)+Li(2 ^{2}S) ($\theta = 90°$ [16]) with calculated spectra, obtained for different choices of the autoionization width $\Gamma(R)$, as shown in fig. 13. The calculations are based on eq. (11) and involve ab initio potentials $V_*(R)$, $V_+(R)$ [13,15]. The theoretical spectra have been convoluted with a spectrometer function of 50 meV fwhm and contain the average over the collision energy distribution.

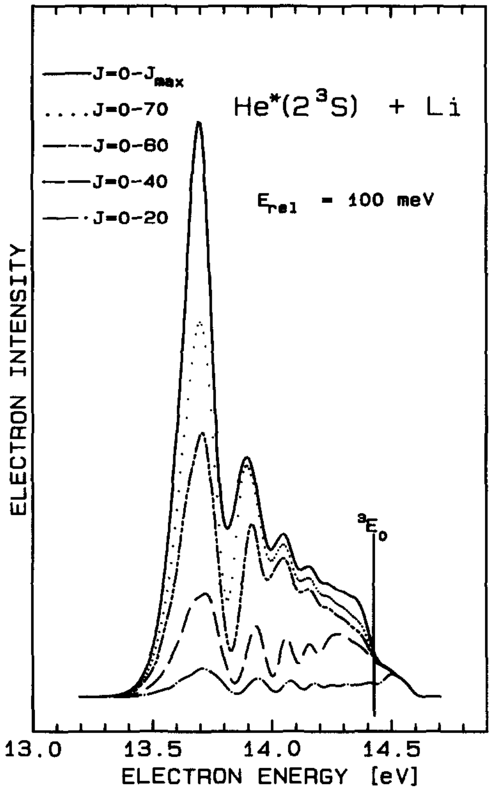

Fig. 15. Evolution of the electron spectrum for He*(2 ^{3}S)+Li(2 ^{2}S) with increasing number of angular momenta J, calculated for the collision energy $E_{rel} = 100$ meV. Ab initio potentials and width [13,15] have been used. The spectra have been convoluted with a spectrometer function of 50 meV fwhm.

$\Delta J > 0$) may be associated with these groups in a way, which depends on electron detection angle. To give an illustrative example, we consider electron emission into the forward (backward) direction (i.e. $\theta \simeq 0°$, 180°) and concentrate on the angular momentum sections $SJ_1 = 71$–80 and $SJ_2 = 41$–60. The insert in fig. 18 shows how these J_* sections are connected with the orientation of the molecular axis in the relevant R range (see also fig. 5a, ref. [13]). The section SJ_1 dominates the main Airy peak (see fig. 15) and does not lead to a directed ΔJ transfer when the electrons are emitted in forward (backward) direction; in contrast, the section SJ_2 contributes in a major way to the first supernumerary Airy peak and leads to a directed angular momentum transfer $\Delta J \approx -4$ ($+4$) for emission into $\theta \simeq 0°$ (180°) (independent of the orientation of the collision plane) [13]. The resulting effect is a larger (smaller) energy separation between the two peaks at $\theta \simeq 0°$ (180°), as reflected by the different shifts in the experimental spectra, when going from $\theta = 45°$ ("forward") to $\theta = 135°$ ("backward"). For further details see the more complete discussion in ref. [13].

In trying to improve on the quantal model calculations done earlier [13], where we have only demonstrated spectra for two particular, directed angular momentum transfers ($\Delta J = \pm 4$), we have now considered different representative angular momentum transfers for each J_* section shown in fig. 15. This

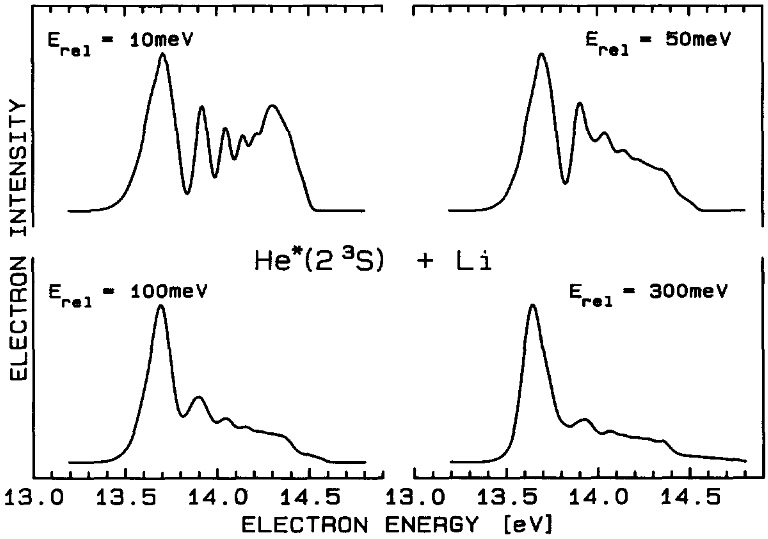

Fig. 16. Collision energy dependence of the electron spectra for He*(2 ^{3}S) + Li(2 ^{2}S), as calculated for four collision energies $E_{\rm rel}$, using ab initio potentials and width [13,15]. The spectra have been convoluted with a spectrometer function of 50 meV fwhm.

procedure is, due to symmetry, approximately correct only for the forward and backward direction. For arbitrary detection angles one has to include the integration over β ($0 \leqslant \beta \leqslant 2\pi$), where β characterizes the collision half planes. Fig. 18 shows the synthesized spectra for forward (a), backward (c), and perpendicular (b) detection; as for the latter ($\theta = 90°$), the symmetries of the collision system and of the angular momentum sections lead to non-directed J transfers only. The chosen J_* dependent values for ΔJ transfer are summarized in table 3; based on a maximum value $|\Delta J| = l = 4$ [13] they are estimated for the respective emission angles shown in the insert of fig. 18 from the relation [13]

$$\Delta J = [m_{\rm Li}/(m_{\rm Li}+m_{\rm He})] R p_{\rm e} \sin\gamma\,. \qquad (15)$$

Here $p_{\rm e}$ is the electron momentum, R is an internuclear distance typical for ionization ($R \approx 6\,a_0$), and γ

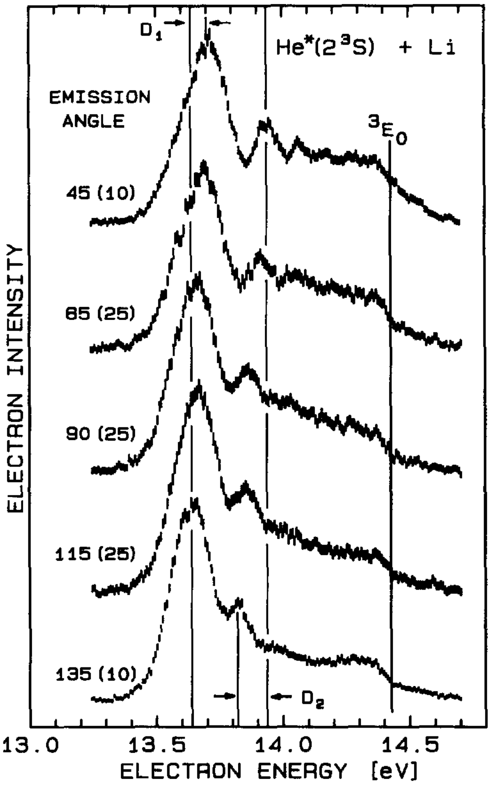

◀ Fig. 17. Experimental electron energy spectra for He*(2 ^{3}S) + Li(2 ^{2}S), measured for five different emission angles θ (average collision energy $\bar{E}_{\rm rel} = 100$ meV; effective energy resolution 40 meV fwhm). The intervals D_1 and D_2 indicate the energy shift of the main and, respectively, the first supernumerary Airy peak, when the electron emission angle increases from $\theta = 45°$ to $\theta = 135°$.

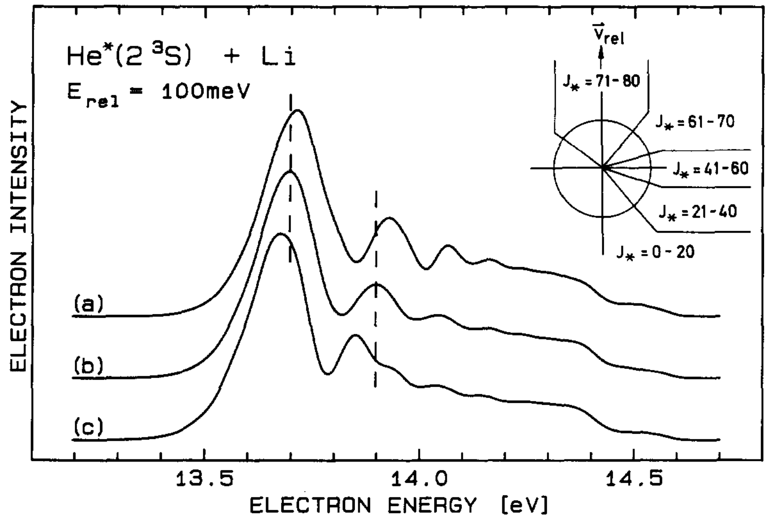

Fig. 18. Model electron spectra for He*$(2\,^3S)$+Li$(2\,^2S)$ at $E_{rel} = 100$ meV, simulating the angular dependence for (a) forward direction ($\theta = 0°$), (b) perpendicular direction ($\theta = 90°$), and (c) backward direction ($\theta = 180°$). The simulation involves J_* dependent ΔJ transfers, as specified in table 3. The insert indicates the J_*-dependent orientation of the molecular axis in the region of internuclear distances, where ionization occurs predominantly.

Table 3
ΔJ transfer in model calculations for the simulation of angle-dependent electron spectra for He*$(2\,^3S)$+Li$(2\,^2S)$ (see fig. 18) (where $|\Delta J|$-ranges are given, an average is performed with equal weights)

J_*	a)	b)	c)
0–20	$\Delta J = -1$	$\lvert\Delta J\rvert \leqslant 3$	$\Delta J = +1$
21–40	$\Delta J = -2$	$\lvert\Delta J\rvert \leqslant 2$	$\Delta J = +2$
41–60	$\Delta J = -4$	$\lvert\Delta J\rvert = 0$	$\Delta J = +4$
61–70	$\Delta J = -2$	$\lvert\Delta J\rvert \leqslant 2$	$\Delta J = +2$
71–80	$\lvert\Delta J\rvert \leqslant 2$	$\lvert\Delta J\rvert \leqslant 3$	$\lvert\Delta J\rvert \leqslant 2$

[a] Forward direction ($\theta = 0°$). [b] $\theta = 90°$.
[c] Backward direction ($\theta = 180°$).

is the electron emission angle relative to the internuclear axis. The vertical dashed lines, centered on the main and first supernumerary Airy peak of spectrum (b) in fig. 18 should help to elucidate the energy shifts due to angular momentum transfer. The main Airy peak shifts by an amount only half of that obtained for the first supernumerary peak, in agreement with the experimental results, shown in fig. 17. The model calculations are not directly comparable with the experimental spectra, since we did not detect electrons emitted in forward or backward direction for reasons of the geometry of the spectrometer and since the measured spectra include always an integration over the angle β. Nevertheless, a qualitatively good agreement is achieved.

We conclude that the recently given, classically motivated picture to explain the angular dependence of the electron energy spectrum by a J_* dependent momentum transfer to the emitted electron is qualitatively, and within this simple model calculation almost quantitatively, able to describe the experimental observations.

4. Conclusions

We have presented new experimental and theoretical results for the simplest Penning ionization systems. Quantum mechanical calculations based on local complex potential theory and on ab initio potential data have shown that the agreement between experiment and theory is good, but not complete. Particularly for the collision system He*$(2\,^3S)$+H a significant discrepancy exists between the width functions, computed with ab initio theory [15,25], and those, determined semi-empirically in fit calculations within the $\Delta J=0$ approximation in the present work and previously [8,9]. In view of this discrepancy we plan to study this fundamental process again in a crossed beam setup with a movable electron spectrometer to detect electrons at different emission angles. The possible ΔJ transfer in the classical picture should be small for the collision system $He^*(2\,^3S)+H$, but the existing differences might be due to other reasons, such as the Coulomb interaction between the emitted electron and the remaining hydrogen ion, which may induce larger $|\Delta J|$. After twenty years of intensive research even for the simplest Penning ionization system there still remain open questions.

Acknowledgement

This work has been supported by the Deutsche Forschungsgemeinschaft through Sonderforschungsbereich 91. We thank N.T. Padial, J.S. Cohen, R.L. Martin and N.F. Lane for providing a preprint of ref. [14] and numerical potential data for the systems $He^*(2\,^3S,\ 2\,^1S)+Na(3\,^2S)$. We acknowledge R. Morgenstern for useful discussions, H.A.J. Meijer for providing the Na oven, and A. Groß for careful secretarial help with the manuscript.

References

[1] H. Hotop and A. Niehaus, Z. Phys. 238 (1970) 452.
[2] H. Hotop, in: Electronic and Atomic Collisions, eds. N. Oda and K. Takayanagi (North-Holland, Amsterdam, 1980) pp. 271ff.
[3] A. Yencha, Electron Spectry. 5 (1984) 197.
[4] H. Morgner, Comments At. Mol. Phys. 21 (1988) 195.
[5] A. Niehaus, Advan. Chem. Phys. 45 (1981) 399; Phys. Rept. 186 (1990) 149.
[6] J. Lorenzen, H. Hotop and M.-W. Ruf, Z. Phys. D 1 (1986) 261.
[7] W.H. Miller, J. Chem. Phys. 52 (1970) 3563.
[8] H. Morgner and A. Niehaus, J. Phys. B 12 (1979) 1805.
[9] H. Waibel, M.-W. Ruf and H. Hotop, Z. Phys. D 9 (1988) 191.
[10] R.J. Bieniek, Phys. Rev. A 18 (1978) 392.
[11] A.P. Hickman and H. Morgner, J. Phys. B 9 (1976) 1765.
[12] M.W. Müller, W. Bussert, M.-W. Ruf, H. Hotop and W. Meyer, Phys. Rev. Letters 59 (1987) 2279.
[13] A. Merz, M.W. Müller, M.-W. Ruf, H. Hotop, W. Meyer and M. Movre, Chem. Phys. Letters 160 (1989) 377.
[14] N.T. Padial, J.S. Cohen, R.L. Martin and N.F. Lane, Phys. Rev. A 40 (1989) 117.
[15] W. Meyer and M. Movre, Z. Phys. D, to be published.
[16] M.-W. Ruf, A. Yencha and H. Hotop, Z. Phys. D 5 (1987) 9.
[17] G. Gerber and A. Niehaus, J. Phys. B 9 (1976) 123; W. Hultzsch, W. Kronast, A. Niehaus and M.-W. Ruf, J. Phys. B 12 (1979) 1821.
[18] J.N.L. Connor and R.A. Marcus, J. Chem. Phys. 55 (1971) 5636.
[19] R.J. Bieniek, J. Phys. B 7 (1974) L 266.
[20] A.Z. Devdariani, V.N. Ostroskii and A. Niehaus, J. Phys. B 18 (1985) L 161.
[21] J.N.L. Connor, D.C. Mackay and K.E. Thylwe, J. Chem. Phys. 85 (1986) 6368.
[22] T.F. O'Malley, Phys. Rev. 150 (1966) 14; 156 (1967) 230.
[23] H. Nakamura, J. Phys. Soc. Japan 26 (1969) 1473; 31 (1971) 575.
[24] W.H. Miller, C.A. Slocomb and H.F. Schaefer III, J. Chem. Phys. 56 (1972) 1347.
[25] A.P. Hickman, A.D. Isaacson and W.H. Miller, J. Chem. Phys. 66 (1977) 1483.
[26] D.M. Jones and J.S. Dahler, Phys. Rev. A 37 (1988) 2916.
[27] D.M. Bishop and L.M. Cheung, J. Mol. Spectry. 75 (1979) 462.
[28] W. Kołos and J.M. Peek, Chem. Phys. 12 (1976) 381.
[29] J.S. Howard, J.P. Riola, R.D. Rundel and R.F. Stebbings, J. Phys. B 6 (1973) L 109.
[30] R.H. Neynaber and S.Y. Tang, J. Chem. Phys. 69 (1978) 4851.
[31] K.L. Bell, A. Dalgarno and A.E. Kingston, J. Phys. B 1 (1968) 18.
[32] J. Tellinghuisen, Advan. Chem. Phys. 60 (1985) 299.
[33] H.A.J. Meijer, Thesis, Rijksuniversiteit Utrecht, The Netherlands (1988).
[34] S. Schohl, M.W. Müller, H.A.J. Meijer, M.-W. Ruf, H. Hotop and H. Morgner, Z. Phys. D, to be published.
[35] J.S. Cohen, R.L. Martin and N.F. Lane, Phys. Rev. A 31 (1985) 152.
[36] D.P. Wang, S.Y. Tang and R.H. Neynaber, J. Phys. B 20 (1987) 1527.